PCCP

Accepted Manuscript

This article can be cited before page numbers have been issued, to do this please use: O. Kurochkin, Y. K. Murugesan, T. Bennett, G. D'Alessandro, Y. Reznikov, B. Tang, G. H. Mehl and M. Kaczmarek, *Phys. Chem. Chem. Phys.*, 2016, DOI: 10.1039/C6CP00116E.

View Article Online
DOI: 10.1039/C6CP00116E

PCCP

ARTICLE

Thermal optical non-linearity of nematic mesophase enhanced by gold nanoparticles – an experimental and numerical investigation

O. Kurochkin,[a] Y. K. Murugesan,[b] T. P. Bennett,[b] G. D'Alessandro,[b] Y. Reznikov,[a] B. J. Tang,[c] G. H. Mehl,[c] and Malgosia Kaczmarek*[d]

Received 00th January 20xx,
Accepted 00th January 20xx

DOI: 10.1039/x0xx00000x

www.rsc.org/

In this work the mechanisms leading to the enhancement of optical nonlinearity of nematic liquid crystalline material through localized heating by doping the liquid crystals (LCs) with gold nanoparticles (GNPs) is investigated. We present some experimental and theoretical results on the effect of voltage and nanoparticle concentration on the nonlinear response of the GNP-LC suspensions. The optical nonlinearity of these systems is characterized by diffraction measurements and the second order nonlinear refractive index, n_2 is used to compare systems with different configurations and operating conditions. A theoretical model based on heat diffusion that takes into account the intensity and finite size of the incident beam, the nanoparticle concentration dependent absorbance of the GNP doped LC systems and the presence of bounding substrates is developed and validated. We use the model to discuss possibilities of enhancing further the optical nonlinearity.

1 Introduction

Materials exhibiting strong nonlinear response to incident light play a vital role in the fields of photonics and optoelectronics owing to their potential in building all-optical systems that can switch or modulate light by light. The anisotropic nature of the liquid crystals (LCs) enhances the optical nonlinearity of these materials by up to nine orders of magnitude comparing to that of isotropic fluids,[1] making these materials suitable for building electro-optical devices. LC channel waveguides capable of all-optical intensity modulation of near infrared light[2] and all-optical switches made of micro-structured fibers filled with LCs[3] and dye doped nematic LCs[4] have already been demonstrated. The significant increase in the magnitude of optical nonlinearity observed in LCs can be achieved through optically controlled spatial variations in refractive indices induced by localized orientational[4,5,6,7] and/or thermal[8] modulations. The susceptibility of LCs to external fields such as electric, magnetic and electromagnetic fields allows the optical nonlinearity of the LCs to be dynamically tuned and controlled by external fields.[13,14,15]

Enhancement of the optical nonlinearity of LCs is achieved through one of the following mechanisms: (I) localized orientational variations induced by (a) doping LCs with dye molecules that undergo photoinduced conformational changes leading to an increased orientational torque on the nematic host when illuminated;[4,5] (b) sandwiching the LCs between inorganic photorefractive crystals that generate surface charge field when illuminated;[6] (c) sandwiching the LCs between photoconducting polymer based substrates that can modulate an applied external field through localized electrical conductance variations when illuminated[7] or (II) localized temperature variations induced by doping the LCs with nanoparticles that can transform radiation at the surface plasmon frequency into heat.[8,9] Due to their surface plasmon resonance which occurs in the visible spectrum, large absorption cross-section, excellent thermal stability[10] and resistance to light induced degradation, gold nanoparticles (GNPs) are better absorbers than dye molecules.

LCs doped with nanoparticles exploit the wavelength specific absorption of light by the nanoparticles. The nanoparticles behave as dispersed nano-heaters that locally modulate the refractive indices of the LCs through spatial temperature variations, improving the nonlinear optical response of the material. For example, nanoparticles dispersed in smectic LCs are known to form stable nanocomposites with large optical nonlinearity and fast response times.[11,12] A cholesteric liquid crystal based plasmonic thermometer that exploits the localized surface plasmon of dispersed gold nanorods have been recently demonstrated.[29] Suspension of GNPs in nematic LCs have been shown to exhibit large thermal nonlinearities with second order nonlinear refractive index, n_2 of up to -2×10^{-5} cm^2W^{-1}.[8] Besides enhancing the optical nonlinearity of the host material, doping the LCs with GNPs improves the electro-optical properties of LCs by increasing the dielectric anisotropy, lowering the optical and electric Freedericksz threshold, improving the thermal stability of the LCs and reducing the switching times.[10] In order to gain insight into the mechanism of thermal optical

[a] Institute of Physics of National Academy of Sciences of Ukraine, Kyiv 03028, Ukraine.
[b] School of Mathematics, University of Southampton, Southampton, SO17 1BJ, United Kingdom.
[c] Department of Chemistry, University of Hull, Hull, HU6 7RX, United Kingdom.
[d] School of Physics, University of Southampton, Southampton, SO17 1BJ, United Kingdom. E-mail: mfk@soton.ac.uk

View Article Online
DOI: 10.1039/C6CP00116E

nonlinearity and to identify the key variables of electro-optical systems comprising LC-GNPs composites, a mathematical model that estimates an effective optical nonlinearity coefficient by solving the thermal diffusion equation in the GNP doped LC layer of the system excluding the presence of bounding substrate was developed by Ouskova et al.[8] This simple model,[8] however, estimated values of second order nonlinear refractive index that were an order of magnitude larger than those determined through experimental measurements. In an attempt to reduce this discrepancy, Acreman et al[13] have proposed an extended model that includes the attenuation of the incident light beams as it traverses the cell. This improved on Ouskova et al's model, but it is not sufficient to reproduce the more extensive data we have measured. Recently,[24] a theoretical model that estimates the photo-induced heat generation by GNPs as a function of dielectric losses, electric field inside the particle and angular frequency of the incident light has been proposed to compute the induced temperature change in LC-GNP systems when illuminated. The dynamics of the birefringence predicted using this model for a temporally varying illumination of LC-GNP composite cell agrees qualitatively with that measured from cross-polarized intensity, but disagrees quantitatively. This, however, is an important issue when modelling the optical response of a LC-GNP composite optical device, because the liquid crystal birefringence is very sensitive to temperature fluctuations. Hence in order to predict accurately the photo-thermal nonlinear response of LC-GNP cells, accurate modelling of the temperature distribution is essential.

In this work we measure the linear and nonlinear properties of a planar cell filled with LC-GNP suspensions of different concentrations. We use these data in an improved thermal model of the device that includes (a) the effect of finite beam width of the pump beams that write the refractive index grating and of the probe beam employed to test it, since only a fraction of the cell volume is illuminated by these beams in our experimental set up, (b) a concentration dependent absorbance coefficient of the LC-GNP suspensions estimated from spectrometric transmittance measurements, (c) the presence of thermally conducting bounding substrates of the cell and (d) the attenuation of pump and probe beams as they traverse the cell, since in LC-GNP suspensions investigated in this work up to 50% of the incident light can be dissipated in propagation. This improved thermal modelling is then validated by quantitatively matching its predictions with the experimentally measured thermal optical nonlinear response at varying pump beam intensities and GNP concentrations.

We also demonstrate, experimentally and numerically, the ability to actively tune and control the photo-thermal nonlinearity of LC-GNP suspensions by reorienting the LC using an applied ac electric field. A model that solves simultaneously the improved and validated heat diffusion equation with the Ericksen-Leslie equations for the field-driven director reorientation of LCs is used to simulate numerically the dynamic tunability of thermal optical nonlinearity in these systems.

Thus the main objectives of this paper are to: demonstrate experimentally the effect of varying the concentration of the GNPs on the magnitude of nonlinear optical response of the LC nanoparticle suspension; determine experimentally the strength of tuneable, optical nonlinearity modulated by an applied ac electric field in E7 nematic LC doped with GNPs; develop a more robust mathematical model to theoretically quantify the nonlinear optical response of these systems with and in the absence of an applied electric field, and finally, validate it using the experimental observations. This model can then be used as a tool to predict and optimize the thermal optical nonlinearity of LC-plasmonic systems.

The organization of the paper is as follows: In section II, we describe the procedure employed for preparing and characterizing the LC cells doped with gold nanoparticles, the experimental system and the methodology used for measuring the diffraction efficiency of the system. In section III, the mathematical model for computing the temperature distribution based on the heat diffusion equation for an absorbing medium and the methodology for theoretical estimation of the diffraction efficiency are presented. Section IV demonstrates experimentally the effect of varying the intensity of the incident light beam, the concentration of the GNPs in the LC cell and the applied ac field on the optical nonlinearity of the system and validates the proposed mathematical model. A review of the results obtained and a discussion of possible extensions to enhance the optical nonlinear response of these systems conclude the paper.

2 Materials and experimental set-up

In this section, the procedure for preparing stable suspensions of gold nanospheres in E7 nematic liquid crystal and building LC cells by sandwiching them between glass slides are presented. The diffraction setup used for experimental characterization of the non-linear optical response of these cells through diffraction efficiency measurements is also detailed.

Cell preparation and characterization

The LC-GNP suspensions were prepared using spherical GNPs of diameter 1.6±0.4 nm synthesized following the procedure reported earlier.[16,17] The nanoparticles were functionalized with short hexanethiol molecules and long laterally linked mesogen molecules to improve their miscibility in LC and the stability of the suspension.[17]

The structure of the LC functionalized GNPs is shown in Figure 1. The Transmission electron microscopy (TEM) investigations that confirm the low polydispersity of the synthesized LC functionalized GNPs are presented in ref. 17. From these data the average particle size of the GNPs has been estimated to be 1.6±0.4 nm.

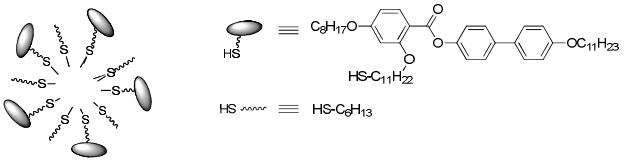

Figure 1. Schematic Representation of the gold liquid crystal nanoparticles used (left) and of the organic groups attached to the nanoparticles.

View Article Online
DOI: 10.1039/C6CP00116E

Prior to the preparation of the LC-GNP suspension, the nanoparticles were dissolved in chloroform (10 mg of GNPs in 1 mL of solvent). The mixture was stirred ultrasonically for 5 min and added to the nematic LC E7 from Merck in the desired weight ratio. This mixture was stirred ultrasonically again and put on a hot-stage at T = 60°C for 30 hours for full evaporation of the solvent. In order to ensure effective removal of the solvent from the GNPs, the controlled evaporation of the mixture was continued until the weight of the dispersion did not vary upon further heating. This procedure allows for preparation of LC-GNPs dispersions in which the weight concentration of the solvent in the matrix is less than $2\times10^{-3.}$ Using this procedure, LC suspensions with different GNP concentration were prepared. The LC suspensions with concentration of GNPs of up to 1.3% by wt. were stable, but for suspensions of higher concentrations sedimentation of nanoparticles was observed. The stability of the LC-GNPs dispersions of GNP concentration 0.2-1.3 wt% has been confirmed by the absence of any visible aggregation and sedimentation. Hence the maximum concentration of GNPs in LC used in the current study was limited to 1.3% by wt. The LC cells were formed by two ITO glass substrates covered with rubbed polyamide polymer layers to promote planar alignment and separated by 50μm thick rod-like polymer spacers. They were filled with the suspensions in the isotropic state. Once fabricated, the absorption spectra of the cells were measured using a Jasco V-570 spectrometer. The absorbance coefficients of LC-GNPs cells of varying nanoparticle concentration are estimated from the absorption spectra and presented in section 4. The alignment of liquid crystal on the polyimide layer on the bounding glass substrate (cell pretilt) and the elastic constant of the GNP doped E7 are determined by fitting the measured cross polarized intensity.[18] The pretilt and splay elastic constant measurements for pure and GNP doped LC cells are also presented in section 4.

The experimental optical setup for the study of the light diffraction in the LC samples is schematically represented in Figure 2. To record dynamic gratings we use two linear polarized Gaussian beams of equal intensities $I_{pump}/2$ from a diode-pumped solid-state laser, indicated by 1 in Figure 2, henceforth referred to as pump beams. Typical pump parameter values are λ_{pump} = 532 nm, I_{pump}=0-100 mW, half-width in the plane of the LC cell 300 μm, The angle of incidence of the two coherent pump beams are such that a diffraction grating of period 50 μm is set up in the LC layer. A low power He-Ne laser (9), wavelength 632.8 nm and beam half-width 300 μm was used as probe beam for the first-order diffraction observation. The probe beam enters the cell at an angle 15° (θ_{probe}) with respect to the normal to the cell. In the experiment, the linear polarization of the pump beam and the test beam was controlled by the polarizers 7 and 10 (see Figure 2) and coincided with the direction of the director of the LC cell (8). The intensity of the first-order diffraction of the test beam was registered by a photodiode (11). The diffraction efficiency was estimated as the ratio of the intensities of the first order diffracted beam and the incident probe beam.

To investigate the dependence of the nonlinearity of the suspension on an external electric field, we applied to the LC cell an AC field with frequency f = 1 kHz.

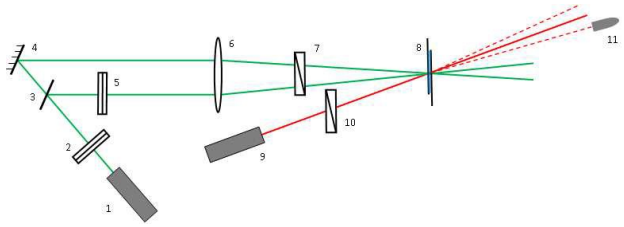

Figure 2. Experimental setup for study of nonlinear properties of LC suspensions with GNPs: 1 – DPSS laser (pump); 2,5 – λ/2 plates (532 nm); 3 – semi-transparent mirror; 4-mirror; 6 – lens; 7,10 – polarizers; 8 – LC cell; 9 - He-Ne laser (probe) beam traversing the cell at an angle θ_{probe} with respect to the cell normal; 11 – photodiode.

3 Modelling the temperature distribution and estimating optical nonlinearity

In order to quantify the thermal optical nonlinearity as a function of system parameters (concentration of GNPs) and operating conditions (intensity of the incident beam and applied AC electric field), we present a model that extends the one developed by Ouskova *et al*.[8] by taking into account the depletion of the pump beam as it traverses the cell[13], the finite width of the pump beam and probe beams and the presence of the LC cell bounding glass substrates. Solving the model yields the temperature distribution in the cell. From the computed change in temperature, the corresponding refractive index grating, the beam phase shift, the far field and ultimately the diffraction efficiency are determined numerically. We assume that the GNPs are dispersed uniformly through the cell and we neglect any thermally driven flow of the LC material.

Computing the spatial temperature distribution

The thermal conductivity of the bounding substrate strongly influences the operating temperature in the cell and hence the amplitude of refractive index modulation. Hence the presence of the bounding glass substrates is taken into consideration while solving the heat diffusion equation. The temperature distribution in the cell is obtained by solving the heat diffusion equation using spectral methods in the LC layer. The analytical Fourier series solution in the bounding glass substrates was used as the boundary condition for the LC layer.

Description	Symbol	Value
Thickness of LC layer	L	50 μm
Thickness of glass substrates	L_G	500 μm
Half-width of pump beam	σ_p	300 μm
Grating period	Λ	50 μm
Thermal conductivity of E7	k_{LC}	0.15 W m^{-1} K^{-1}
Thermal conductivity of glass	k_{GL}	1 W m^{-1} K^{-1}
Ambient temperature	T_A	295.15 K

Table 1. Typical parameter values used to determine the liquid crystal temperature profile.

View Article Online
DOI: 10.1039/C6CP00116E

We model the cell as a LC layer that extends infinitely in the x and y-direction and has thickness 2L in the z-direction, with $-L \le z \le L$. The LC layer is sandwiched between two glass layers each of thickness L_G. The absorption of the light by the suspension leads to a change of the temperatures T_{GL}, T_{LC}, T_{GR} in the glass substrate on the left, the LC layer and the glass substrate on the right respectively. For a system with absorbance coefficient α, illuminated by two coherent Gaussian beam of intensity I_{pump}, the temperature change can be found by solving the heat diffusion equation in the cell. Typical parameter values are given in Table 1 and Table 5.

The heat diffusion equation for the LC domain is

$$k_{LC}\nabla^2 T_{LC} = -\alpha I_{pump} e^{-\alpha z} e^{-\frac{x^2+y^2}{\sigma_p^2}} \left[1+\cos(qx)\right], \quad -L \le z \le L, \tag{1a}$$

where $q = 2\pi/\Lambda$ is the wave number of the grating of period Λ and σ_p is the half-width of the pump beam.

In the glass substrates the heat diffusion equations are

$$\nabla^2 T_{GL} = 0; \qquad -L - L_G \le z \le -L, \tag{1b}$$

$$\nabla^2 T_{GR} = 0; \qquad L \le z \le L + L_G. \tag{1c}$$

These equations are complemented by the boundary conditions that the temperature and the heat flux are continuous at the interfaces between the glass substrates and the LC and that the temperature at the glass-air interfaces is equal to the ambient temperature:

$$T_{GL}(-L) = T_{LC}(-L); \tag{2a}$$

$$T_{LC}(+L) = T_{GR}(+L); \tag{2b}$$

$$\frac{\partial T_{LC}}{\partial z}(-L) = \kappa \frac{\partial T_{GL}}{\partial z}(-L); \tag{2c}$$

$$\frac{\partial T_{LC}}{\partial z}(+L) = \kappa \frac{\partial T_{GR}}{\partial z}(+L); \tag{2d}$$

$$T_{GL}(-L-L_G) = T_A; \tag{2e}$$

$$T_{GR}(L+L_G) = T_A, \tag{2f}$$

where κ is the ratio of the thermal conductivity of glass to that of the LC and T_A is the ambient temperature.

Solving the heat diffusion equations semi-analytically in Fourier space enables to recast eqns. (1b) and (1c) as boundary conditions on the equation in the LC layer eqn. (1a). Let $\tau_{GL}, \tau_{LC}, \tau_{GR}$ be the Fourier transform in the x,y plane of the temperature profiles T_{GL}, T_{LC}, T_{GR} respectively and $\mathbf{k} = (k_x, k_y)$ be the Fourier wave vector with modulus $k = |\mathbf{k}|$. Using this notation, eqn. (1) can be written as:

$$\frac{d^2}{dz^2}\tau_i - k^2\tau_i = f_i(k_x, k_y, z), \tag{3}$$

where i={GL, LC, GR} is an index to identify the layer and f_{GL} and $f_{GR} \equiv 0$ while f_{LC} is the Fourier transform of the right hand side of the eqn. (1a). Eqn. (3) is then solved along with the Fourier transform of the boundary conditions in eqn. (2).

For the glass substrate on the right hand side, solving eqn. (3) with i=GR that satisfies the boundary condition eqn. 2(f), we obtain

$$\tau_{GR}(z) = A_{GR}\sinh\left[k(L_G + L - z)\right]. \tag{4}$$

Substituting the Fourier transform of the boundary condition eqn. (2b) into eqn. (4), we obtain

$$\tau_{GR}(z) = \frac{\tau_{LC}(L)}{\sinh(kL_G)}\sinh\left[k(L_G + L - z)\right]. \tag{5}$$

We substitute the derivative of eqn. (5) in eqn. (2d) to obtain a Robin boundary condition on τ_{LC} at z=L:

$$\frac{d}{dz}\tau_{LC}\Big|_{z=L} = -\frac{kK}{\tanh(kL_G)}\tau_{LC}\Big|_{z=L}. \tag{6}$$

Similarly the heat diffusion equation for the glass substrate on the left hand side can be transformed to Robin boundary condition on τ_{LC}:

$$\frac{d}{dz}\tau_{LC}\Big|_{z=-L} = \frac{kK}{\tanh(kL_G)}\tau_{LC}\Big|_{z=-L}. \tag{7}$$

Therefore, the temperature profile inside the LC layer can be obtained by solving eqn. (3) with i=LC and boundary conditions eqns. (6) and (7). Once the solution in Fourier space is obtained by taking the inverse Fourier transform the spatial change in temperature in the cell is obtained.

Computing the LC alignment in the cell

At zero voltage the alignment of the liquid crystal is uniform across the cell. This is no longer true if an AC voltage is applied to the cell. To model this effect, we represent the liquid crystal alignment by the angle θ that the director field makes with the z-axis. As the elastic constants and dielectric permittivity of the liquid crystal are a function of temperature, the alignment of the liquid crystal in general depends on all spatial coordinates. However, we make the assumption that the spatial modulation in the (x,y)-directions induced by thermal effect is small in comparison to the voltage induced changes in the z-direction and consider the alignment as a function of this last coordinate only. Its values as a function of space are obtained by solving the Ericksen-Leslie equation

$$\left[1-\delta_2\cos(2\theta)\right]\frac{d^2\theta}{dz^2} + \delta_2\sin(2\theta)\left(\frac{d\theta}{dz}\right)^2 + \delta_1\sin(2\theta)\left(\frac{d\phi}{dz}\right)^2 = 0, \tag{8}$$

where δ_1 is the scaled electrostatic coupling coefficient and δ_2 is the normalized elastic anisotropy of the LC (see Table 2).

Table 2. Typical elastic and electrostatic[26] parameters for E7 nematic LC.

$\delta_1 = \frac{\varepsilon_0(\varepsilon_\parallel - \varepsilon_\perp)}{K_3 + K_1}$ $\alpha_L = \frac{\varepsilon_\parallel - \varepsilon_\perp}{\varepsilon_\parallel + \varepsilon_\perp}$	AC dielectric permittivity parallel to the director: $\varepsilon_\parallel = 19.67$ AC dielectric permittivity perpendicular to the director: $\varepsilon_\perp = 5.31$
$\delta_2 = \frac{K_3 - K_1}{K_3 + K_1}$	Splay elastic constant: K_1. The values used are indicated in Table 4. Bend elastic constant: K_3=17.1 pN (from Merck data sheet).

The director field is determined uniquely by specifying its values at the cell boundaries (pretilt angles). The electrostatic potential ϕ in eqn. (8) is obtained by solving the Maxwell's equations for electrostatics.

View Article Online
DOI: 10.1039/C6CP00116E

$$\frac{d}{dz}\left\{\left[1-\alpha_L \cos(2\theta)\frac{d\phi}{dz}\right]\right\}=0, \quad (9)$$

where α_L is a measure of the dielectric anisotropy (see Table 2).

Finally, we assume that these equations are valid both for pure and doped liquid crystals. This is reasonable because the variations in dielectric permittivities of the LC due to addition of nanoparticles is negligible as the volume fraction of the nanoparticles in the cells is very small, of the order 10^{-4}.[27]

Computing the diffraction efficiency

The spatial temperature change distribution T_{LC} obtained by solving eqn. (1) and alignment θ obtained by solving eqns. (8) and (9) are used to determine the refractive index grating using an extended Cauchy model.[21]

Since the local optical axis of the LC is along its director, the effective refractive index seen by the polarisation component of the probe beam in the director plane is given by: [25]

$$n_{eff}(T_{LC},\theta)=\frac{n_e(T_{LC})n_o(T_{LC})}{\sqrt{n_e(T_{LC})^2\sin^2(\theta)+n_o(T_{LC})^2\cos^2(\theta)}}, \quad (10)$$

Where n_e and n_o are the temperature dependent extraordinary and ordinary refractive indices of the LC. For nematic LC phase investigated in this study, the temperature dependent refractive indices can be modelled using an extended Cauchy model,

$$n_e(T)=A-BT+\frac{2\Delta n_0}{3}S(T), \quad (11a)$$

$$n_o(T)=A-BT-\frac{\Delta n_0}{3}S(T), \quad (11b)$$

where T is the temperature in Kelvin and A, B and Δn_0 are wavelength dependent fitting parameters. S(T) is the scalar order parameter as a function of temperature obtained using Haller's approximation,[22]

$$S(T)=\left(1-\frac{T}{T^{\dagger}}\right)^{\gamma}, \quad (12)$$

where $T^{\dagger}$ and γ are also fitting parameters. The fitting parameters in eqns. (11) and (12) were determined by fitting E7 refractive index data[21] at the probe beam wavelength, λ_{probe} (633nm) and are listed in Table 3.

Table 3. Fitting parameters of Cauchy model for temperature dependent refractive indices of E7 nematic LC.

Parameter	Fitted values
A	1.7485
B	5.3362×10^{-4}
Δn_0	0.3523
$T^{\dagger}$	329.43 K
γ	0.2161

The variation of the ordinary and extraordinary refractive indices of E7 at the probe wavelength as a function of temperature corresponding to the fitting parameters listed in the table 3 are plotted in figure 3. It can be seen that the extraordinary refractive index is considerably more sensitive to temperature than the ordinary refractive index. This observation emphasizes the necessity for an accurate thermal modelling for predicting the optical nonlinearity of these systems.

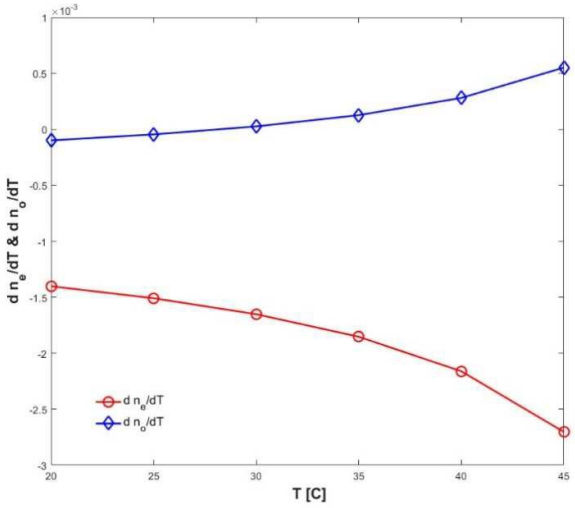

Figure 3. Variation of the ordinary and extraordinary refractive indices of E7 as a function of temperature.

From the spatial temperature and orientation distribution, the corresponding refractive index grating is obtained using the Extended Cauchy model detailed in eqns. (10-12). The total phase shift of the incident probe beam of wavenumber k resulting from this refractive index grating is determined using the expression

$$\Delta\Phi=\frac{k}{\cos(\theta_{probe})}\int_{-L}^{L} n_{eff}(x,y,z)\,dz \quad (13)$$

The phase shift modulates the phase of the probe beam. Assuming that its phase at input is uniform, the probe beam amplitude at output is

$$E_{out}(x,y)=e^{-\frac{(x^2+y^2)}{\sigma_{pr}^2}}e^{i\Delta\Phi} \quad (14)$$

where σ_{pr} is the probe beam half-width. The spatial Fourier transform of this field yields the far-field diffraction pattern:

$$\tilde{E}_{out}(k_x,k_y)=\frac{1}{2\pi}\int_{-\infty}^{+\infty}\int_{-\infty}^{+\infty} E_{out}(x,y)e^{-i(k_x x+k_y y)}dxdy. \quad (15)$$

We define the diffraction efficiency as the ratio of the intensities of the first diffracted order and the incident probe beam:

$$\eta=\frac{\frac{1}{2}\left(\int_{\Omega(k=q)}|\tilde{E}_{out}|^2dk_xdk_y+\int_{\Omega(k=-q)}|\tilde{E}_{out}|^2dk_xdk_y\right)}{\left(\sum_{n=-1}^{+1}\int_{\Omega(k=nq)}|\tilde{E}_{out}|^2dk_xdk_y\right)e^{\frac{\alpha_{probe}2L}{\cos(\theta_{probe})}}}, \quad (16)$$

where $\Omega(k)$ is a neighbourhood of the point (k,0) in the far field, chosen to be large enough to contain all the energy of the corresponding diffracted order. The terms in the numerator gives the averaged intensity of the two diffracted first order beams. The denominator computes the incident probe beam intensity by summing the computed intensity of the diffracted beams assuming the intensity of the beams of diffraction orders higher than 1 are negligible. The exponential term in the denominator accounts for the loss in intensity of the probe beam as it traverses the cell at an angle θ_{probe}. This computed value of the diffraction efficiency is used

View Article Online
DOI: 10.1039/C6CP00116E

to validate the model by matching it with experimentally measured diffraction efficiency.

4 Results

In this section we present our main experimental and modelling results: (i) we have fitted cross-polarised intensity measurements to determine the pretitlt at the polyimide alignment layers and the splay elastic constant for the doped and undoped cells; (ii) we have used spectrometric measurements to determine the absorbance coefficient of the LC cells as a function of the GNP concentration; (iii) we have measured and computed the diffraction efficiency and optical nonlinearity as a function of the pump beam intensity, concentration of GNPs and applied electric field.

Pretilt and elastic constants

To determine the average pretilt angles and liquid crystal splay elastic constant we have fitted the values of the cross-polarised intensity measured using a standard setup. The light of a He-Ne laser (632.8 nm) entered the cell at normal incidence; the input beam was polarised at 45° to the rubbing direction and the output beam passed through a second polariser with optical axis orthogonal to the first. A 1 kHz AC voltage was applied to the cell, and the output beam intensity was measured as a function of its amplitude and subsequently fitted using the model in equations (8-9). The experimental and best-fit curves for a pure and doped LC are plotted in Figure 4, while the fitted values of the pretilt and splay elastic constant are presented in Table 4. The errors in determining these variables through fitting are calculated by estimating the deviation when the cell thickness was varied by 10% with respect to the cell gap created by the spacers (50μm).

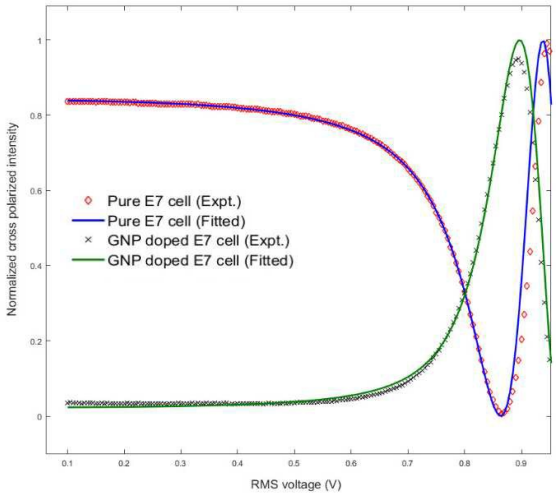

Figure 4. Experimental and fitted normalized cross-polarized intensity for LC cell doped with 1% by wt. of GNP and pure E7 cell.

Table 4. Fitted values of average pretilt and splay elastic constant for GNP doped and undoped cells.

Material	Pretilt on PI surfaces (deg)	Splay elastic constant (pN)
Pure E7	1.783±0.075	11.54±0.07
E7 + 1 wt% GNP	1.451±0.065	11.13±0.09

The fitted parameters are in good agreement with literature values for pretilt[28] (typically between 1° and 2.1° for various LC systems) and the value of splay elastic constant for E7 (11.7 pN) as specified in Merck data sheet. The fitted values for the pretilt and the splay elastic constant are used in the simulations to determine the spatial distribution of alignment of the LC in the cells. The bend elastic constant, which plays an important role only at high values of the applied voltage, is not of significance to this study where the voltage applied is of the order of few volts. Hence the bend elastic constant has not been fitted and the value reported in Merck data sheet has been used.

Absorption spectra

Since the absorption of incident radiations is a function of nanoparticle concentration and wavelength of the incident light, the absorbance coefficient at the resonant wavelength of gold is determined by measuring the fraction of unpolarised, incident light transmitted through the medium when no voltage is applied to the cell. Since the alignment of LCs is uniform inside the cell and the nanoparticles are present in very low volume fractions, scattering and reflection losses have been considered negligible. Figure 5 shows the optical density of the suspensions as a function of wavelength computed from spectrometric data. The relationship between optical density, absorbance coefficient and the transmission data obtained from spectrometry is given by

$$D = 2\alpha L = -\ln(T), \qquad (17)$$

where D is the optical density and T is the fractional transmittance of incident light defined as the ratio of the output and incident beam intensities. This computation of absorbance coefficients attributes all the light absorbed by the cell to be transduced to heat by the GNPs doped LC layer, assuming comparatively negligible absorption by the glass substrates, ITO electrodes and the alignment layers.

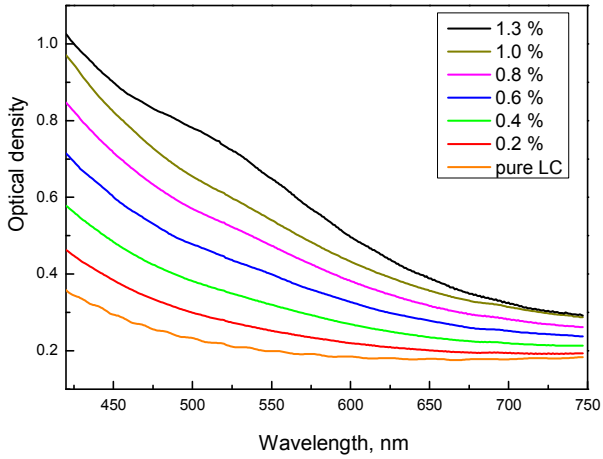

Figure 5. Absorption spectrum of LC suspensions with concentration of GNPs ranging from 0% - 1.3% wt.

View Article Online
DOI: 10.1039/C6CP00116E

The fact that the extinction spectra do not exhibit a pronounced Surface Plasmon resonance peak can be attributed to the small size of the particles in suspensions of very low volume fraction. This observation is in accordance with experimental measurements and theoretical predictions of absorption spectra of gold nanoparticle for dilute suspensions and nanosize GNPs as presented in refs. 19,20. The measured values of absorbance coefficient for the undoped LC and suspensions of GNPs of varying concentration in nematic LCs are listed in Table 5.

Table 5. Absorbance coefficients of pure and GNP doped E7 at 532 nm.

Concentration of GNPs in E7 (wt.%)	Absorbance coefficient α at 532nm [cm^{-1}]
0 (Pure E7)	42.14
0.2	53.25
0.4	67.95
0.6	84.9
0.8	101.6
1.0	116.08
1.3	140.13

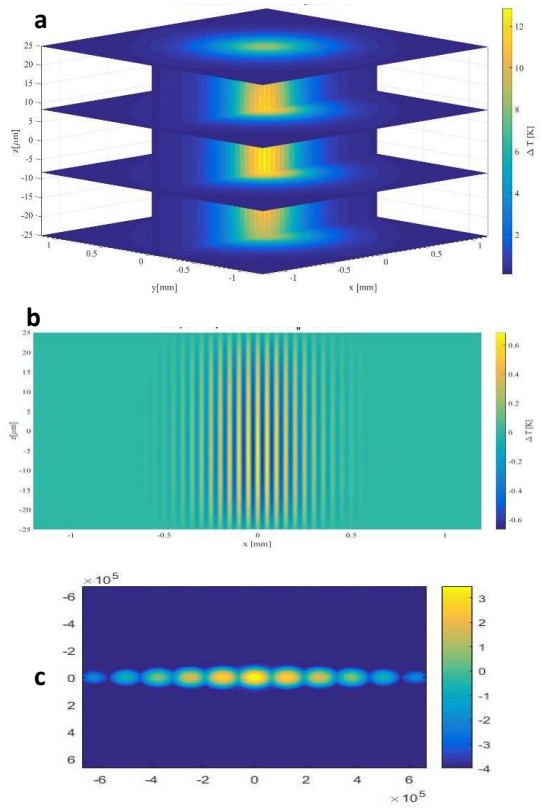

Figure 6. Estimated temperature distribution and resulting diffraction intensity pattern: (a) computed change in temperature in degrees Kelvin estimated in a layer of E7 doped with 1% by wt. of GNPs and bound between two glass substrates when illuminated by a pump beam of intensity 19.5 W/cm^2; (b) y=0 cross-section of the periodic temperature modulation corresponding to the temperature distribution in figure 6(a); (c) the intensity profile of the diffracted probe beam corresponding to the refractive index grating resulting from the temperature modulation shown in figure 6(b).

Effect of varying the pump beam intensity

From eqn. (1a) it is evident that the temperature change due to heating of the nanoparticles by the incident light is a linear function of the intensity of the pump beams. In order to demonstrate this dependence, the diffraction efficiency is measured as a function of pump beam intensity following the experimental procedure detailed in section 2.

Figure 6 shows the temperature distribution and diffracted beam intensity profile estimated following the procedure detailed in section 3. The typical change in temperature estimated by solving eqn. (1) in a layer of E7 doped with 1% by wt. of GNPs and bound between two glass substrates when illuminated by a pump beam of intensity 19.5 W/cm^2 is presented in figure 6(a). The maximum change in temperature estimated for this system is 12.85 K. Figure 6(b) shows a cross-section in the plane y=0 of the periodic modulation in temperature change resulting due to the cosine term in eqn. 1(a). The resulting diffraction pattern corresponding to the same cell parameters and operating condition is depicted in figure 6(c). From the diffracted intensity profile presented in figure 6(c), the diffraction efficiency of the E7-1% GNPs by wt. can be computed using eqn. (16).

Figure 7 shows the variation of the square root of the diffraction efficiency with intensity of the incident beam predicted by eqn. (16) following the procedure detailed in section 3, for a cell filled with 1% by wt. GNP doped E7 nematic LC. The agreement between the experimental measurement and the theoretical prediction verifies the ability of our model to predict the diffraction efficiency of a LC-GNP cell. This confirms the necessity to include the effect of finite size of the incident beam and the presence of bounding substrates in order to accurately predict the experimentally observed optical nonlinearity in these systems.

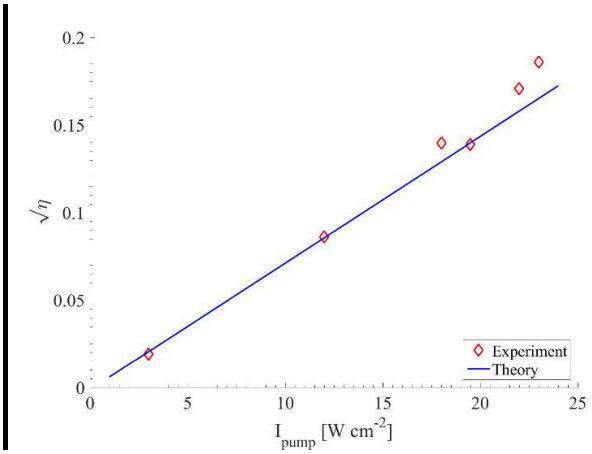

Figure 7. Diffraction efficiency η as the function of pump beam intensity for LC cells filled with 1% by wt. GNP doped E7. The theoretical curve was obtained using the parameters in Tables 1, 3 and 5.

Varying the concentration of GNPs

From the model eqn. (1a), it can be seen that another key variable that can affects the optical nonlinearity of these systems is the absorbance coefficient of the system. In order to investigate the effect of this variable and optimize the system, the concentration of

View Article Online
DOI: 10.1039/C6CP00116E

the GNPs in LC was varied from 0 to 1.3% by weight. The cell made of pure, undoped E7 does not exhibit measureable diffraction of the probe beam and hence the thermal optical nonlinearity of the pure liquid crystal is negligible compared to that of the cells with GNP doped LCs.

In order to provide a parameter to help comparing the diffraction efficiencies of systems of varying concentrations and operating conditions, we define the second order nonlinear refractive index n_2 as

$$n_2 \approx \frac{\sqrt{\eta}\lambda_{probe}\cos(\theta_{probe})}{2I_{pump}\pi L}. \quad (18)$$

This is the equivalent nonlinearity that would give rise to the same diffraction efficiency in a generic nonlinear system in the Raman-Nath regime in the limit of small η. It is a measure of nonlinearity independent of the intensity of incident beam and facilitates isolating the effect of concentration and applied electric field on optical nonlinearity. This nonlinear refractive index is related to the modulation of effective refractive index in the liquid crystal implicitly through eqns. (10-16). The temperature induced modulation of the effective refractive index [eqns. (10-12)] causes a phase modulation [eqn. (13)] that diffracts a probe beam with strength measured by the diffraction efficiency parameter η [eqn. (16)]. In eqn. (18), the increased propagation distance of the probe beam due to the tilting of the cell with respect to the probe beam is taken into account by dividing the cell thickness by cosine of θ_{probe}, the angle between the probe beam and the cell normal.

The effective optical nonlinearity coefficients as a function of concentration of GNPs, determined from experimentally measured and theoretical computed diffraction efficiency values, are plotted in figure 8. The theoretical estimation of the second order nonlinear refractive index plotted in the figure is obtained by estimating the temperature distribution in LC cells by solving the eqn. (1) in combination with the absorbance coefficients listed in Table 5 and then using eqns. (10-16,18). The experimental data depicted in figure 8 are obtained from the measured diffraction efficiency in LC-GNPs systems of varying GNP concentration and using eqn. (18) to compute the corresponding n_2 values. The figure shows a generally good agreement between experimental and theoretical values. At very low concentrations of GNPs, the second order nonlinear refractive index predicted by the model is slightly higher perhaps due to the model estimating a higher temperature in the LC layer. This discrepancy possibly arises from attributing all the light absorbed by the cell to the LC layer while computing the absorbance coefficients. At higher concentrations of GNPs, the light absorbed by the substrates, the electrodes and the alignment layers are negligible comparing to that absorbed by the GNPs doped LC layer, hence the experimental observations agrees well with the model predictions. However, at low concentration of GNPs when the light transduced to heat by the LC layer doped with GNPs is comparable to or lower than that absorbed by the substrates, the electrodes and the alignment layers, the model predicts a slightly higher values of n_2. From the figure 8, we can see that the optical nonlinearity can be further increased by increasing the concentration of the GNPs. However with the GNPs used in this study, we are limited to a maximum n_2 coefficient of -3.1×10^{-5} cm^2/W, as the suspension of concentrations higher than 1.3% by weight are not stable.

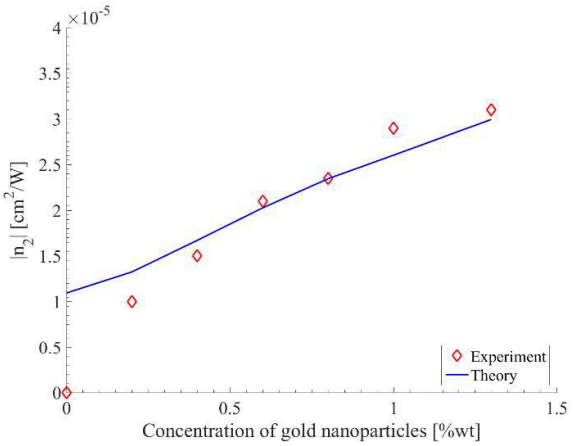

Figure 8. The second order nonlinear refractive index n_2 as the function of concentration of GNPs in the LC for an incident pump beam intensity of 19.5 W/cm^2

Effect of applied field

As mentioned in Section 2 and shown in figure 3, the change of the E7 extraordinary refractive index with temperature is an orders of magnitude larger than that of the ordinary refractive index. As pointed out in ref. 13, this difference in magnitude opens up the possibility of dynamically controlling the optical nonlinearity by varying the director orientation. In the two cases presented in figure 7 and 8, the director is aligned along the optical axis and consequently the largest possible optical nonlinearity for a given concentration and pump beam intensity is observed. By reorienting the director perpendicular to the optical axis, the resulting optical nonlinearity is reduced considerably. The significant enhancement of optical nonlinearity due to the doping of LC with GNPs demonstrated through experimental observations in figure 8 makes the LC-GNPs systems more effective candidates for dynamically tuning the optical nonlineaity by applying an external field compared to pure LC. In this work, we reorient the LC by applying an ac electric field. The director orientation as a function the applied AC voltage is computed using the procedure detailed in section 3.

The effective optical nonlinearity coefficient as a function of applied voltage computed from experimentally and theoretical computed diffraction efficiency are plotted in figure 9. These curves demonstrate the possibility of tuning the second order nonlinear refractive index of these systems by applying an external AC voltage. At very low voltages, the LC is aligned at the pretilt angle and has an effective refractive index close to that of the extraordinary refractive index. As the Fréedericksz threshold voltage is reached, the LC orientation changes drastically towards the ordinary refractive index and the second order nonlinear refractive index reduces to 0. While the experiment exhibits a drastic change to zero optical nonlinearity, the model predicts a more gradual reduction. We attribute this discrepancy to the increased light scattering in the LC that we have observed near the Fréedericksz transition and has also been reported in Ref. 23. This phenomenon is not taken into account by our model.

View Article Online
DOI: 10.1039/C6CP00116E

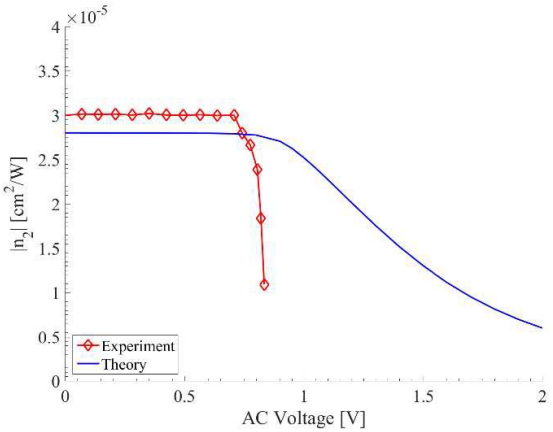

Figure 9. The second order nonlinear refractive index n_2 as the function of applied AC voltage in the LC doped with 1% wt. GNPs and illuminated by pump beam of intensity 22 W/cm^2.

5 Conclusions

This paper demonstrates the possibility for enhancing the optical nonlinearity of nematic LCs by doping them with gold nanoparticles that act as localised nanoheaters when illuminated by light. We have experimentally shown the effect of varying the concentration of the GNPs on the magnitude of nonlinear optical response of the LC nanoparticle suspension and demonstrated the tuneable strong cubic optical nonlinearity modulated by an applied ac electric field in E7 nematic LC doped with GNPs. We have developed and validated a mathematical model to theoretically quantify the nonlinear optical response of these systems and validate it using the experimental observations.

Some possible ways to enhance the optical nonlinear response further and limitations to these systems have been discussed as follows:
It is evident from eqn. 1(a) that the temperature change in these systems under illumination has two components: a modulated component that is a function of the grating of period Λ and a uniform component that decides the operating temperature T_{LC}. Hence the second order nonlinear refractive index and diffraction efficiency can be greatly improved by increasing the maximum modulation of the temperature change and/or the operating temperature as dn_e/dT increases sharply with increase in T as shown in figure 3. These changes can be achieved by increasing the concentration of the GNPs and by using a substrate of lower thermal conductivity than glass that results in higher system temperature.

The theoretical and experimental observations presented in Figure 7 indicate that increasing the concentration of GNPs increase both the modulated component of temperature change and the system temperature owing to increase in source of localized heating. In our work we are able to more than double the optical nonlinearity by doping pure LCs with GNPs of concentration up to 1.3% by weight. However, the suspension becomes unstable upon further increasing the concentration. Thus using nanoparticle systems that exhibit higher solubility of GNPs[10] can further enhance optical nonlinearity. For nanosize particles, the surface plasmon resonance effect increases considerably as a function of particle size, due to the contributions from higher order resonance modes as the size of the particles increase.[19,20] Thus using GNPs of larger size will increase the absorbance coefficient and hence will increase the optical nonlinearity of these systems. By using a material of lower thermal conductivity such as polymeric substrates to build the LC cells, the system temperature (T_{LC}) can be increased resulting in increased optical nonlinearity. For example, by replacing the glass substrates with polymeric substrates of lower thermal conductivity such as PET ($k_{PET} \approx k_{LC}$), the effective optical nonlinearity predicted by our validated model for 1% by wt. GNPs doped LC systems is amplified by up to 4 times and the diffraction efficiency can be amplified by 10 times. However, this method has the disadvantage that the system will be operating much closer to the clearing point and hence degree of alignment of the LC will drastically decrease as the system temperature approaches the nematic-isotropic transition temperature. This can lead to nucleation of defects resulting in scattering losses that can reduce the experimentally observed optical nonlinearity.

Thus identifying an optimal operating temperature at which a balance between high optical nonlinearity and reasonably well aligned nematic LC phase can be attained and using higher concentration of larger GNPs than that used in this study can allow attaining higher optical nonlinearity in these GNPs doped LC cells.

Acknowledgements

The authors would like to thank the EPSRC Research Grant EP/J006920/1 and COST Action funding MP1205 for supporting this research. BJT acknowledges the EU for funding through contract 228455.

References

1. L. Marrucci, *Liquid Crystals Today*, 2002, **11,** 6.
2. A. d'Alessandro, R. Asquini, M. Trotta, G. Gilardi, R. Beccherelli and I.C. Khoo, *Applied Physics Letters*, 2010, **97,** 093302.
3. J. Tuominen, H. Hoffrén and H. Ludvigsen, *Journal of the European Optical Society-Rapid publications*, 2007, **2,** 07016.
4. I.-C. Khoo, J.-H. Park and J.D. Liou, *Journal of the Optical Society of America. B*, 2008, **25,** 1931.
5. I. Janossy and T. Kosa, *Optics letters*, 1992, **17,** 1183.
6. D. Evans and G. Cook, *Journal of Nonlinear Optical Physics & Materials*, 2007, **16,** 271.
7. O. Buchnev, A. Dyadyusha, M. Kaczmarek, V. Reshetnyak and Y. Reznikov, *Journal of the Optical Society of America B*, 2007, **24,** 1512.
8. E. Ouskova, D. Lysenko, S. Ksondzyk, L. Cseh, G. Mehl, V. Reshetnyak and Y. Reznikov, *Molecular Crystals and Liquid Crystals*, 2011, **545,** 123/[1347].
9. A.Y.-G. Fuh, C.-Y. Lin, M.-S. Li and H.-C. Lin, *Journal of Physics D: Applied Physics*, 2012, **45,** 445104.
10. J. Mirzaei, M. Urbanski, H.-S. Kitzerow and T. Hegmann, Philosophical *Transactions of the Royal Society of London A: Mathematical, Physical and Engineering Sciences*, 2013, **371,** 20120256.
11. A. Lyashchova, D. Fedorenko, Y. Garbovskiy, G. Klimusheva, T. Mirnaya and V. Asaula, *Liquid Crystals*, 2013, **40,** 1377.

View Article Online
DOI: 10.1039/C6CP00116E

12. P. de Melo, A. Nunes, L. Omena, S. do Nascimento, M. da Silva, M. Meneghetti and I. de Oliveira, *Physical Review E*, 2015, **92,** 042504.
13. A. Acreman, M. Kaczmarek and G. D'Alessandro, *Physical Review E*, 2014, **90,** 012504.
14. R. Pratibha, K. Park, I. Smalyukh and W. Park, *Optics express*, 2009, **17,** 19459.
15. Q. Liu, Y. Cui, D. Gardner, X. Li, S. He and I.I. Smalyukh, *Nano letters*, 2010, **10,** 1347.
16. J. Dintinger, B.J. Tang, X. Zeng, F. Liu, T. Kienzler, G.H. Mehl, G. Ungar, C. Rockstuhl and T. Scharf, *Advanced Materials*, 2013, **25,** 1999.
17. L. Cseh and G.H. Mehl, *Journal of the American Chemical Society*, 2006, **128,** 13376.
18. K.R. Daly, Light–matter interaction in LC cells, in, University of Southampton, 2011.
19. K. Yamada, K. Miyajima and F. Mafuné, *The Journal of Physical Chemistry C*, 2007, **111,** 11246.
20. S. Kubo, A. Diaz, Y. Tang, T.S. Mayer, I.C. Khoo and T.E. Mallouk, *Nano letters*,2007, **7,** 3418.
21. J. Li, C.-H. Wen, S. Gauza, R. Lu and S.-T. Wu, *Journal of Display Technology*, 2005, **1,** 51.
22. Haller, *Progress in solid state chemistry*, 1975, **10,** 103.
23. P. Allia, C. Oldano, P.T. Valabrega and L. Trossi, *Physica scripta*, 1991, **44,** 388.
24. L. Pezzi, L. De Sio, A. Veltri, T. Placido, G. Palermo, R. Comparelli, M.L. Curri, A. Agostiano, N. Tabiryan and C. Umeton, *Physical Chemistry Chemical Physics*, 2015, **17,** 20281.
25. P. De Gennes and J. Prost, The physics of liquid crystals, 1993, *Oxford University Press, New York.*
26. M. Clark, E. Raynes, R. Smith and R. *Journal of Physics D: Applied Physics*, 1980, **13,** 2151.
27. T.P. Bennett, G. D'Alessandro and K.R. Daly, *Physical Review E*, 2014, **90,** 062505.
28. S.-H. Paek, C.J. Durninga, K.-W. Lee and A.Lien, *Journal of Applied Physics*, 1998, **83(3)**, 1270.
29. G. Palermo, L. De Sio, T. Placido, R. Comparelli, M.L. Curri, R. Bartolino And C. Umeton, *Molecular Crystals and Liquid Crystals*, 2015, **614**, 93.